Journal of Nuclear Materials 480 (2016) 129–137

Contents lists available at ScienceDirect

Journal of Nuclear Materials

journal homepage: www.elsevier.com/locate/jnucmat

Displacement rate and temperature equivalence in stochastic cluster dynamics simulations of irradiated pure α-Fe

Aaron Dunn [a, b], Brittany Muntifering [a, c], Rémi Dingreville [a], Khalid Hattar [a], Laurent Capolungo [b, d, *]

[a] Sandia National Laboratories, Albuquerque, 87185 NM, USA
[b] George W. Woodruff School of Mechanical Engineering, Georgia Institute of Technology, Atlanta, 30332 GA, USA
[c] Northwestern University, Chicago, 60208 IL, USA
[d] Material Science and Technology Division, MST-8, Los Alamos National Laboratory, Los Alamos, 87545 NM, USA

ARTICLE INFO

Article history:
Received 7 March 2016
Received in revised form
10 August 2016
Accepted 15 August 2016
Available online 20 August 2016

Keywords:
Radiation damage
Temperature
Dose rate
Cluster dynamics

ABSTRACT

Charged particle irradiation is a frequently used experimental tool to study damage accumulation in metals expected during neutron irradiation. Understanding the correspondence between displacement rate and temperature during such studies is one of several factors that must be taken into account in order to design experiments that produce equivalent damage accumulation to neutron damage conditions. In this study, spatially resolved stochastic cluster dynamics (SRSCD) is used to simulate damage evolution in α-Fe and find displacement rate/temperature pairs under 'target' and 'proxy' conditions for which the local distribution of vacancies and vacancy clusters is the same as a function of displacement damage. The SRSCD methodology is chosen for this study due to its computational efficiency and ability to simulate damage accumulation in spatially inhomogeneous materials such as thin films. Results are presented for Frenkel pair irradiation and displacement cascade damage in thin films and bulk α-Fe. Holding all other material and irradiation conditions constant, temperature adjustments are shown to successfully make up for changes in displacement rate such that defect concentrations and cluster sizes remain relatively constant. The methodology presented in this study allows for a first-order prediction of the temperature at which ion irradiation experiments ('proxy' conditions) should take place in order to approximate neutron irradiation ('target' conditions).

1. Introduction

Ion irradiation has long been used as a method for experimentally simulating damage in metals expected from neutron irradiation in reactor environments, due to the lower costs, increased safety, and faster completion of such experiments [1–8]. Although ion irradiation can cover a wide range of displacement rates and total doses, the displacement rates in typical ion irradiation experiments intended to simulate neutron irradiation range from 10^{-2}–10^{-5} dpa$\cdot$s^{-1}, while neutron irradiation displacement rates range from 10^{-7}–10^{-12} dpa$\cdot$s^{-1} [2–5,9,10]. Therefore, ion irradiation experiments are often carried out at higher temperatures than the neutron irradiation conditions they are simulating in order to produce similar defect concentrations and size distributions.

Several experimental and theoretical studies have investigated the temperature shift required to achieve similar results at different displacement rates, using metrics for equivalent damage such as swelling and segregation in alloys [2–4,8,11–15]. However, experimental studies are typically limited in the range of irradiation conditions tested, while most theoretical studies have used simplified models of damage accumulation that do not account for important factors such as displacement cascades [2,4,11,13,14]. Recently, a more advanced modeling study by Xu et al. [15] has overcome many of these obstacles using a complex cluster dynamics tool and displacement cascades resulting from both ion and neutron damage. In this study, a computational method which addresses some of these limitations is introduced to aid in the estimation of experimental parameters such as irradiation temperature in order to simulate accelerated aging of metals using charged particles as a proxy for neutron damage.

* Corresponding author. George W. Woodruff School of Mechanical Engineering, Georgia Institute of Technology, Atlanta, 30332 GA, USA.
E-mail address: laurent@lanl.gov (L. Capolungo).

http://dx.doi.org/10.1016/j.jnucmat.2016.08.018
0022-3115/

This paper presents the use of a multi-scale damage accumulation tool, called spatially resolved stochastic cluster dynamics (SRSCD) [16], to simulate both Frenkel pairs (caused by electrons and light ions) and displacement cascade damage (caused by heavy ions and neutrons) over a wide range of displacement rates and temperatures. SRSCD is a computationally efficient methodology for simulating damage accumulation in spatially resolved domains while enabling formation of defect clusters and simulation of displacement cascade damage. This method is an extension of the stochastic cluster dynamics (SCD) for damage accumulation in homogeneous media [17]. The data produced by these simulations is then used to estimate the temperature shift required to produce similar damage content when the displacement rate is shifted by several orders of magnitude. Therefore, damage production is measured during irradiation for two cases:

1. **Target conditions:** for example, irradiation at $T_T = 20$ °C or $T_T = 200$ °C at the 'target' displacement rate ϕ_T.
2. **Proxy conditions:** irradiation at the 'proxy' displacement rate ϕ_P and temperature T_P required to produce similar radiation damage accumulation to the 'target' conditions.

The temperature shift $\Delta T_P = T_P - T_T$ required when changing from displacement rate ϕ_T to ϕ_P is presented for rates ranging from 10^{-2}–10^{-8} dpa•s^{-1} for both types of irradiation. The above damage conditions represent a conceptual attempt to model the temperature shift required during ion irradiation (represented here by the 'proxy' conditions) in order to reproduce damage caused by neutron irradiation (represented here by the 'target' conditions). As the intent of this study is to focus primarily on two variables, displacement rate and temperature, the irradiation conditions simulated are not intended to represent realistic irradiation conditions. As such, several variables such as primary knock-on atom (PKA) spectra and nonuniform irradiation profiles are not treated here. Therefore, the results presented in this study are intended only as a first-order approximation of the differences between neutron and ion damage conditions due to changes in temperature and displacement rate, and the reported correspondence between displacement rate and particle flux is for illustration purposes only.

2. Methodology

Irradiation of α-Fe is simulated using SRSCD for three damage scenarios: (1) Frenkel pair damage to 10^{-2} dpa in 100 nm thin films using a $100 \times 50 \times 50$ nm domain with free surfaces in the *x*-direction treated as perfect sinks with zero defect concentration and periodic boundary conditions in the *y*- and *z*-directions, similar to the methodology of Li et al. [18]; (2) cascade damage created by 20 keV primary knock-on atoms (PKAs) to 10^{-2} dpa inside bulk α-Fe using a $100 \times 100 \times 100$ nm domain with periodic boundary conditions in all directions; and (3) cascade damage created by 20 keV PKAs to 10^{-2} dpa in α-Fe thin films with thickness ranging from 50 to 200 nm, using the same boundary conditions as case (1). Note that the use of 20 keV PKAs in this study is intended as a first approximation for displacement damage from neutron or charged particle sources capable of inducing displacement cascades, independent of incident particle energy. This places effective limits on the upper and lower bound of particle energies for which these conditions are a good approximation. These boundary conditions have been used in previous studies to simulate both ion irradiation of thin films and neutron irradiation of bulk iron with SRSCD [19,20]. In all cases, radiation damage is distributed uniformly throughout the computational domain. Although a non-uniform distribution of displacement damage would be expected in the case of thin films, the damage profiles predicted by Stopping Range of Ions in Matter (SRIM) simulations [21] (see below) are relatively uniform through the thickness of the material.

The three damage scenarios listed above correspond to approximations of three different experimental environments: case (1) corresponds to damage conditions in electron and light ion irradiation experiments, case (2) corresponds to neutron irradiation conditions, and case (3) corresponds to heavy ion irradiation of thin films. All allowed defects and reaction rates are the same as in previous SRSCD simulations of damage accumulation in α-Fe [20]. The defect types included in the simulations in this work are the following:

1. *Single vacancies and self-interstitials:* These defects are treated as spherical and migrate in three dimensions with diffusion rates given by a standard Arrhenius law, $D = D_0 e^{-\frac{E_m}{k_b T}}$. They are allowed to form clusters and annihilate with defects of the opposite type.
2. *Small mobile vacancy and self-interstitial clusters:* Vacancy and self-interstitial clusters size 2–4 are treated as spherical clusters that diffuse in 3D. Pairs of clusters are allowed to combine, annihilate, and undergo thermal emission of point defects.
3. *Larger immobile vacancy clusters:* Vacancy clusters size 5 or greater are assumed to be immobile, spherical defects. These defects can interact with mobile defects via clustering or annihilation, and can emit single vacancies.
4. *Interstitial dislocation loops:* Self-interstitial clusters size 5 or greater are assumed to form circular dislocation loops [22]. These dislocation loops can be mobile and diffuse in 1D. Mobile dislocation loops can become immobile if two dislocation loops meet and form a junction [23] or if they encounter a trap.

Migration and binding energies E_m and E_b as well as diffusion prefactors D_0 required to compute reaction rates are taken from atomistic simulations in α-Fe [22,24]. A full description of migration and binding parameters used in this study is given in Appendix A. Cases (1) and (3) can be seen as a first order approximation of defect accumulation in a nanocrystalline material with grain boundaries that act as sinks, with grain size on the order of the film thickness.

For case (1), displacement damage (in dpa) is calculated by dividing the number of implanted Frenkel pairs by the number of atoms in the simulated volume. For cases (2) and (3), displacement damage is calculated in a similar fashion, by dividing the total number of displaced atoms in stable defects formed in cascades by the number of atoms in the simulated volume. To generate cascade damage inputs in SRSCD, displacement cascades created by 20 keV PKAs are taken from atomistic simulations performed by Stoller et al. [25,26]. The cascades are first annealed for 10 ps in the OKMC code MMonCa [27] in order to allow only reactions triggered automatically by proximity to occur. By doing so, the defects input into SRSCD include all clusters formed during the cascade itself. Note that the use of OKMC in this process does not imply long timescale simulations in which thermally activated migration and clustering reactions occur; OKMC is simply used here as a tool for identifying defect clusters created in atomistic simulations. The simulations described in cases (1)–(3) are repeated at displacement rates ranging from 10^{-8}–10^{-2} dpa•s^{-1}, spanning the majority of experimental neutron and ion irradiation dose rates. The average concentration of vacancies and vacancy clusters over ten simulations for Frenkel pair damage and five simulations for cascade damage at each displacement rate and temperature combination is used as a metric to compare results between different irradiation conditions. The choice of vacancy concentration as a metric for equivalent damage accumulation is motivated in this work by the relatively large number of such defects remaining compared to self-interstitial clusters at the end of the simulations.

Fig. 1 demonstrates the methodology used in this study to

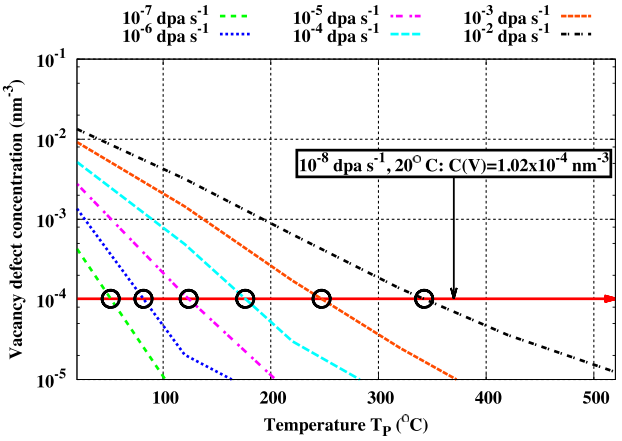

Fig. 1. Method used to identify equivalent temperatures for irradiation at various displacement rates in order to simulate room temperature Frenkel pair implantation in 100 nm α-Fe thin films at 10^{-8} dpa·s^{-1}. The intersection of each curve with the red arrow (black circles) indicates the displacement rate equivalent temperature. (For interpretation of the references to color in this figure legend, the reader is referred to the web version of the article.)

compute the 'proxy' temperature T_P at displacement rate ϕ_P required to produce equivalent damage to room temperature irradiation ($T_T = 20$ °C) at the 'target' displacement rate ϕ_T. The irradiation conditions used in Fig. 1 correspond to damage scenario (1) described above, in which a 100-nm Fe thin film is irradiated to 10^{-2} dpa. The irradiation time of each data point in Fig. 1 is determined by the time required to reach 10^{-2} dpa at the given dose rate. This methodology is used for all irradiation conditions, and is outlined in the following steps:

1. The concentration of vacancy defects (single vacancies and vacancy clusters) at $[T_T,\phi_T]$ is first computed (red arrow).
2. This result is compared to the concentrations found at other displacement rates ϕ_P as a function of temperature T_P.
3. An estimate is made of the temperature T_P at which the concentration of vacancies produced at dose rate ϕ_P is the same as at T_T and ϕ_T (black circles on Fig. 1). The temperature shift $\Delta T_P = T_P - T_T$ required to produce the same vacancy content at both displacement rates is then reported.
4. This process is repeated using displacement rates $\phi_T,\phi_P \in [10^{-8},10^{-2}]$ dpa·s^{-1}.

Therefore, the increase or decrease in temperature ΔT_P required to produce equivalent radiation damage to room-temperature irradiation at a different displacement rate is found for a two-dimensional input space of displacement rates ϕ_T and ϕ_P, using vacancy concentration as a metric for equivalent damage. Note that in order to find the temperature shift required by changing the displacement rate, all other variables associated with the model such as the geometry of the simulated sample are the same for simulations at target and proxy conditions. Therefore, a direct comparison between ion irradiation near free surfaces (e.g. in thin films) and neutron damage in a bulk material is not made in this study.

3. Results

3.1. Temperature shifts ΔT_P

Fig. 2 shows maps of the temperature shift ΔT_P found using the above methodology for the cases of Frenkel pair irradiation in

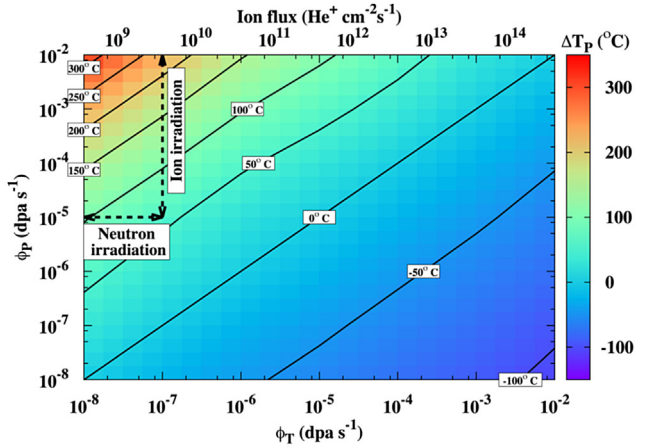

(a) Frenkel pair damage in 100 nm Fe thin film, reference temperature $T_T = 20°$ C

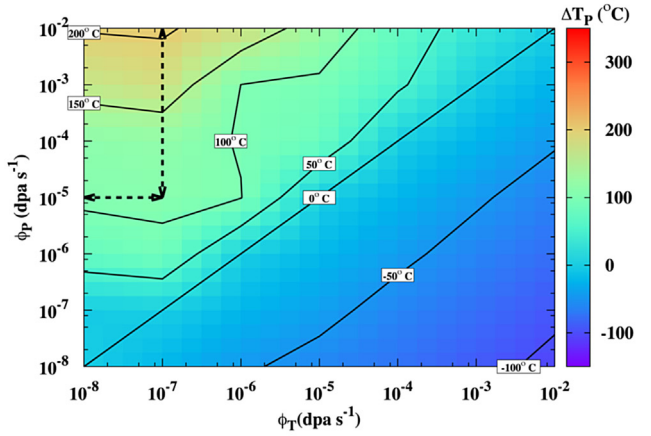

(b) Cascade damage in bulk Fe, reference temperature $T_T = 20°$ C

Fig. 2. Temperature shift ΔT_P from room temperature (20 °C) required when changing from displacement rate ϕ_T to ϕ_P to produce equivalent vacancy content. Arrows indicate displacement rates that correspond to the use of ion irradiation to reproduce damage caused by neutron irradiation. Results are shown for Frenkel pair implantation in 100 nm thin films (2a) and cascade damage in bulk α-Fe (2b).

100 nm α-Fe (2a) thin films and displacement cascade damage in bulk α-Fe (2b). Frenkel pair irradiation in bulk α-Fe was also tested, but results for the estimated temperature shift ΔT_P are similar to the case of thin films despite the fact that the presence of free surfaces in the thin film simulations decreased the defect content. In both cases, increasing the proxy displacement rate ϕ_P requires an increase in proxy irradiation temperature T_P to achieve equivalent radiation damage. Several differences can be seen between the cases of Frenkel pair and cascade damage in Fig. 2a and b. A greater temperature shift ΔT_P is required to reproduce radiation damage accumulation at $\phi_T = 10^{-8}$ dpa·s^{-1} when $\phi_P = 10^{-2}$ dpa·s^{-1} for Frenkel pair damage than cascade damage. However, during cascade damage the dependence of temperature T_P on ϕ_T and ϕ_P is much more irregular than for the case of Frenkel pair damage. For example, a temperature shift ΔT_P of approximately 100 °C is necessary when $\phi_T = 10^{-6}$ dpa·s^{-1} and $\phi_P = 10^{-5}$ dpa·s^{-1}, whereas for the case of Frenkel pair irradiation the value of ΔT_P is below 50 °C for the same values of ϕ_T and ϕ_P. In addition, for the case of cascade implantation, little difference is seen between $\phi_T = 10^{-8}$ and $\phi_T = 10^{-7}$ dpa·s^{-1}, implying that no additional defect mobility is achieved by slowing down the displacement rate below

10^{-7} dpa·s^{-1} at room temperature.

The irregularity in the contour line representing $\Delta T_P = 100$ °C in Fig. 2b is due to statistical fluctuations in the SRSCD output resulting from the kinetic Monte Carlo framework of the method as well as the fact that the region where $\Delta T_P \approx 100$ °C is quite broad for the case of cascade damage. When $\Delta T_P = 100$ °C above room temperature, small defects and defect clusters are quite mobile and therefore do not remain in the system, instead annihilating or clustering to form larger, immobile clusters (see Table A.1). However, the temperature is not high enough for these larger immobile clusters to dissociate. This leads to a quasi-steady-state system in which the damage accumulation is only weakly dependent on displacement rate for the range of rates studied here. Quantification of the statistical uncertainty in the values of ΔT_P found in this study is warranted, but requires an exhaustive statistical study that is outside the scope of this work. Further discussion of the source of these irregularities is given in Appendix B.

Although the displacement rates reported in this study are in units of dpa·s^{-1}, experimental measures of radiation dose are typically in units of particle flux, or particles cm^{-2} s^{-1}. In experimental studies using ion irradiation, the relationship between displacement rate and ion flux is dependent on factors such as the incident ion mass and energy and the sample thickness. In Fig. 2a, the estimated ion fluxes required to generate the displacement rates studied in this work have been estimated using the Stopping Range of Ions in Matter (SRIM) code [21] for the case of irradiation of a 100 nm Fe thin film with 50 keV helium ions. The dpa measurement was estimated using SRIM recoil simulations under the "detailed calculation with full damage cascade" mode and zero tilt angle between the ion beam and the thin film's surface normal [21]. These fluxes are shown at the top of the chart in units of He^+ cm^{-2} s^{-1}. The ion energy chosen is within the range of typical experimental capabilities [28–30] and generates a relatively flat damage profile with very little remaining helium in the system while still producing damage in the form of Frenkel pairs. Fluxes are not reported for the case of cascade damage in bulk Fe (Fig. 2b) because these simulations are intended to match neutron damage conditions. As a reference for ion irradiation experiments, the ion fluence required to generate 1 dpa of displacement damage in a 100 nm Fe thin film (averaged through the thickness of the film) has also been computed using SRIM for a range of incident ion energies for the cases of helium and self-ion irradiation. These results are shown in Fig. 3. A minimum is reached near 20 keV for helium ion irradiation and 200 keV for self-ion irradiation as the irradiation regime shifts from implantation, in which most incident ions stop in the thickness of the foil, to a regime in which most incident ions pass through the foil, creating a flatter damage profile. Note that these results are only intended as a rough guide, as results depend on film thickness. Therefore a direct comparison between thin film irradiation with ions and bulk irradiation with neutrons is not made here, as the intent of this work is to investigate the impact of changing the displacement damage rate only while keeping all other irradiation parameters equal.

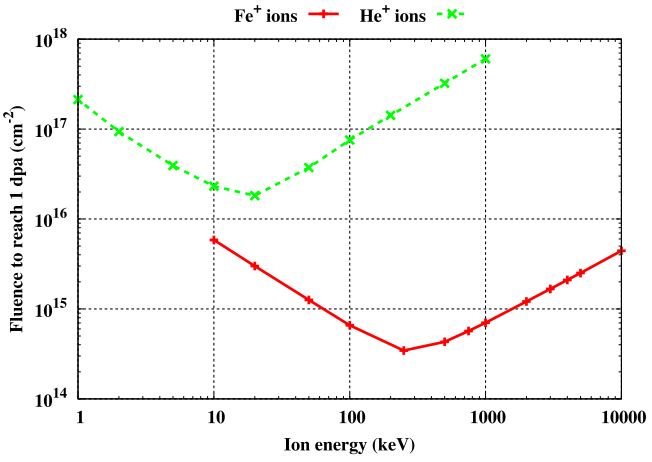

Fig. 3. Incident ion fluence (ions· cm^{-2}) required to produce 1 dpa of displacement damage in 100 nm Fe thin foils as a function of ion energy in SRIM simulations. Displacement damage is averaged over the thickness of the foil.

The region of interest corresponding to the use of ion irradiation to reproduce damage caused by neutron irradiation at room temperature is shown by arrows in Fig. 2a and b. Although these regions represent a small subset of the entire range of displacement rates ϕ_T and ϕ_P simulated in this study, the temperature shift required to reproduce damage at displacement rates associated with neutrons using ion irradiation varies by 100–200 °C within this region for cascade and Frenkel pair damage, respectively. This result emphasizes the necessity of correctly choosing irradiation temperature based on the proxy and target irradiation conditions.

3.2. Effect of film thickness

To test the effect of the density of planar sinks such as grain boundaries and free surfaces on the temperature shift ΔT_P, Fig. 4 shows temperature shifts using cascade damage and the same irradiation conditions as presented above for thin films with thickness 50 nm and 200 nm. The free surfaces of the thin films are treated as perfect sinks. Although some differences in ΔT_P can be seen when film thickness changes from 50 nm to 200 nm in Fig. 4a and b, the region of interest for using ion irradiation to reproduce damage expected from neutron irradiation (indicated by arrows) is similar for both thicknesses. This region is also similar to the case of cascade damage in bulk α-Fe shown in Fig. 2b. This result indicates that for films with thickness greater than 50 nm, film thickness is not a primary variable when determining temperature shift ΔT_P required when changing displacement rates.

As in Fig. 2, the estimated ion fluxes required to generate the displacement rates in Fig. 4 have been computed using the SRIM code [21] for the case of irradiation of 50–200 nm Fe thin films with 3 MeV Fe^+ ions, similar to the approach of Li et al. [18] for simulating displacement damage in molybdenum thin films irradiated with krypton ions. These fluxes are shown at the top of Fig. 4a and b. Self-ion irradiation is a commonly used technique for producing displacement cascades in experiments due to the fact that no other atomic species are implanted into the thin film [31,32]. The ion energy chosen here is within the range of typical experimental capabilities [29,33] and produces a relatively flat damage profile in SRIM simulations of damage in thin films. Due to the greater ion mass and energy, the number of displaced atoms created by each incident ion is much greater than in the case of helium irradiation in Fig. 2a, and the ion flux is correspondingly lower for the same displacement rate ϕ. In addition, the fluxes reported are slightly different between Fig. 4a and b due to the difference in thickness of the two simulated thin films.

3.3. Effect of increasing target temperature T_T

So far, all results presented in this study assume that the 'target' irradiation conditions are at room temperature. Although some experimental neutron irradiation is carried out at temperatures below thermal reactor temperatures [34], it is important to understand how the temperature shifts calculated in this model change when the reference temperature for irradiation T_T is elevated above room temperature. This case is shown in Fig. 5 for

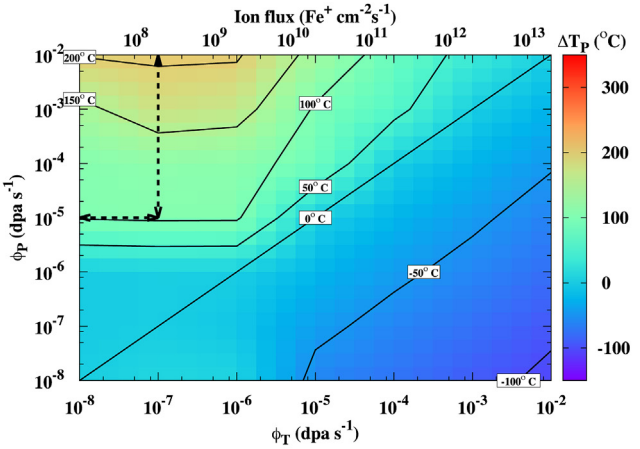

(a) Cacscade damage in 50 nm thin film, reference temperature T_T = 20° C

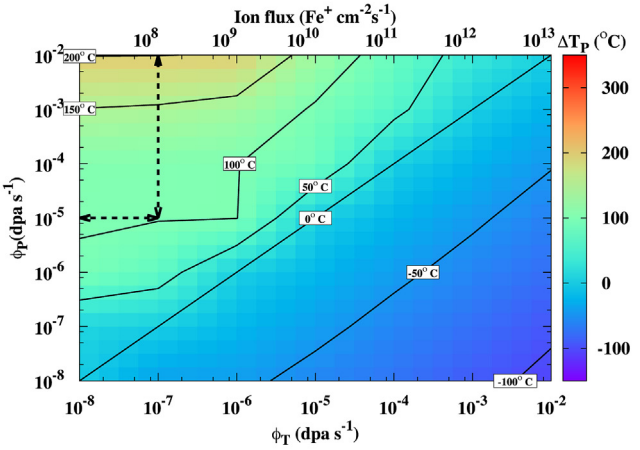

(b) Cascade damage in 200 nm thin film, reference temperature T_T = 20° C

Fig. 4. Temperature shift ΔT_P at displacement rates ϕ_P required to reproduce room-temperature irradiation results at target displacement rates ϕ_T for cascade damage in Fe thin films with thickness ranging from 50 to 200 nm.

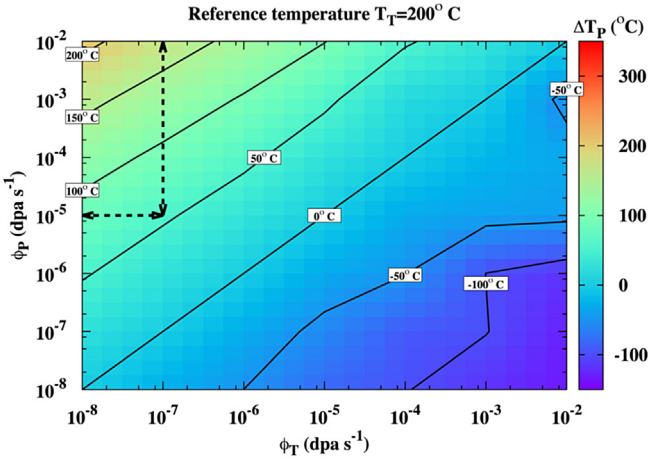

(a) Target temperature T_T = 200° C

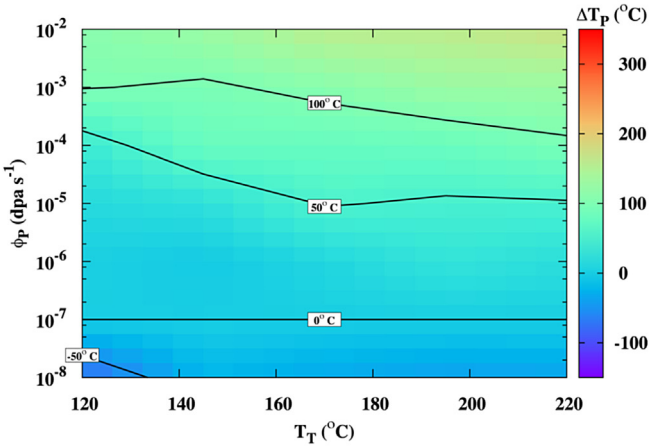

(b) Target displacement rate $\phi_T = 10^{-7}$ dpa·s^{-1}

Fig. 5. Temperature shift ΔT_P at displacement rates ϕ_P required to reproduce irradiation results for cascade damage in bulk Fe at target temperatures above room temperature: (5a) target temperature T_T = 200 °C, and (5b) target temperature 120° ≤T_T ≤ 220° C with target displacement rate $\phi_T = 10^{-7}$ dpa·s^{-1}.

cascade damage in bulk α-Fe. Results are shown for simulations with variable target displacement rate ϕ_T and target temperature T_T = 200 °C (Fig. 5a) and simulations with variable target temperature T_T and target displacement rate $\phi_T = 10^{-7}$ dpa·s^{-1} (Fig. 5b). Several differences are seen between the predicted temperature shift ΔT_P for the cases of T_T = 200 °C (Fig. 5a) and T_T = 20 °C (Fig. 2b); most notably, the temperature shift required when $\phi_P > \phi_T$ is much more regular in Fig. 5a due to the increased mobility of defects at the higher target irradiation temperature.

The dependence of ΔT_P on T_T when ϕ_T is fixed is investigated in more detail in Fig. 5b for 120° ≤T_T ≤ 220 °C. The temperature shift ΔT_P shown in Fig. 5b changes as a function of T_T, indicating that displacement rates alone are not sufficient to determine the required temperature shift ΔT_P in an experiment. Note that cascade damage at $\phi_T = 10^{-7}$ dpa·s^{-1} produces similar damage content in SRSCD for temperatures 20° ≤T_T ≤ 120 °C, resulting in a poor estimate of ΔT_P due to statistical scatter. Therefore, results in this lower temperature range are not included in Fig. 5b. Overall, 'target' irradiation temperature T_T is an important parameter in determining the temperature shift required in the proxy environment ΔT_P to reproduce damage when displacement rates are varied. A higher value of T_T corresponding to reactor temperatures (approximately 400 °C) was not used in this study due to complete annealing of the simulated material at very high temperatures. To capture damage accumulation at these higher temperatures, a more advanced model is needed that can capture effects such as void diffusion and coalescence, defect accumulation at grain boundaries, and the impact of alloying elements and transmutation products such as helium.

3.4. Comparison of defect cluster sizes

The use of the concentration of vacancies and vacancy clusters as a metric for comparing irradiation at different displacement rates and temperatures assumes that the overall defect state in materials irradiated at equivalent temperatures and displacement rates will be the same. However, temperature changes do not lead to uniform changes in defect behaviors because the activation energies for various defect binding and migration reactions are not uniform. Therefore, irradiation at different displacement rates using the temperature shift ΔT_T shown in Fig. 2 may result in differences in damage evolution not measured by the vacancy concentration metric used in this work.

In order to test the quality of vacancy concentration as a metric

for displacement rate equivalent temperature, profiles of vacancy cluster concentrations as a function of cluster size are shown in Fig. 6 for irradiation temperatures T_T and T_P when the proxy and target displacement rates ϕ_T and ϕ_P are different by several orders of magnitude. Profiles are also shown using high displacement rates ϕ_P while leaving temperature $T_P = 20^\circ$ C as a reference. Note that these figures are intended to show the level of correspondence between equivalent displacement rate and temperature pairs in SRSCD simulations, rather than to indicate experimentally measurable cluster sizes. In all cases, the clusters shown in Fig. 6 are smaller than the approximately 1.5 nm resolution limit of typical TEM measurement [18]. Fig. 6a shows a comparison between 10^{-6} dpa·s^{-1} and 10^{-2} dpa·s^{-1} irradiation with Frenkel pairs, and Fig. 6b shows a comparison between 10^{-8} dpa·s^{-1} and 10^{-2} dpa·s^{-1} irradiation with displacement cascades. In both cases, when using the value of T_P calculated in Fig. 2, cluster profiles are very similar for irradiation at temperature and displacement rate pairs $[T_T, \phi_T]$ and $[T_P, \phi_P]$. Although only cluster sizes up to 30 are shown in Fig. 6, cluster profiles show good agreement up to the largest defect sizes produced in these simulations. By contrast, simply irradiating at the higher displacement rate ϕ_P while leaving temperature $T_P = 20^\circ$ C leads to a significant underestimate of the average cluster size in the simulations. This indicates that vacancy and vacancy cluster concentrations are a good metric for comparing defect accumulation at different displacement rates and temperatures. Similar results were observed using $T_T = 200^\circ$ C, indicating that increased cluster dissociation activity that occurs at these higher temperatures does not impair the quality of the match between cluster profiles of equivalent displacement rate/temperature pairs.

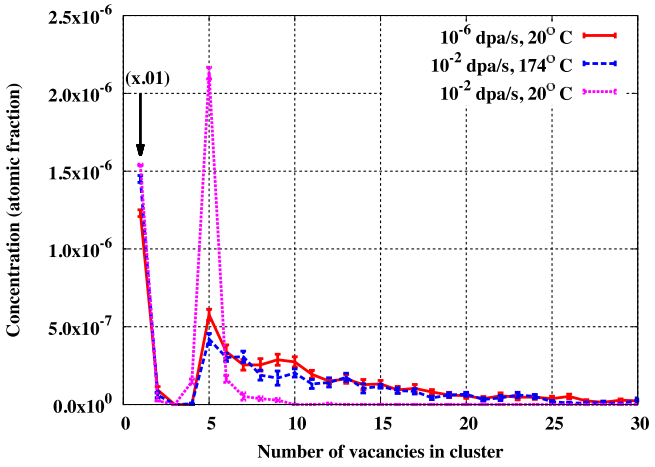

(a) Frenkel pair damage

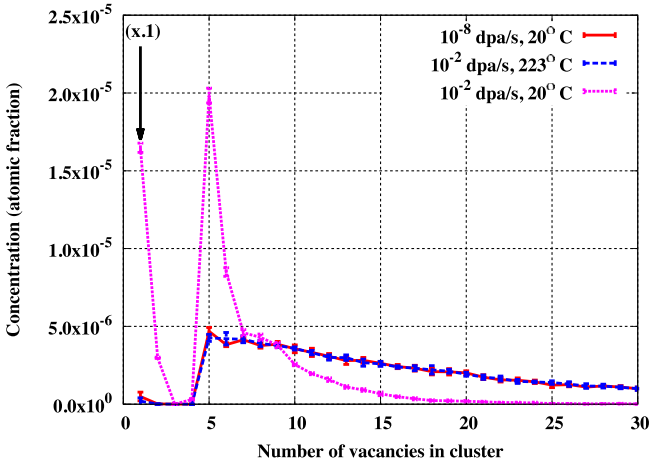

(b) Cascade damage

Fig. 6. Comparison of profiles of vacancy cluster size for simulations at equivalent temperatures: (6a) Frenkel pair damage comparing displacement rates of 10^{-2} and 10^{-6} dpa·s^{-1}, and (6b) cascade damage comparing displacement rates of 10^{-2} and 10^{-8} dpa·s^{-1}. The first two values of the results at room temperature and 10^{-2} dpa·s^{-1} are multiplied by 0.01 and 0.1 in 6a and 6b, respectively, for better visualization (indicated by arrows).

4. Discussion

Although this study addresses the effect of compensating for changes in displacement rate by changing temperature in irradiated α-Fe, there are several other differences between ion and neutron irradiation that could have an impact on damage accumulation that are not treated here. In this study, all displacement cascades are created by 20 keV PKAs, while in ion and neutron irradiation conditions displacement cascades have different ranges of PKA energies [10,35]. Some studies have suggested that when controlling for dpa rate, damage accumulation due to different cascade energies is similar [20,36,37], but nonetheless differences between ion and neutron damage could occur due to the different cascade energy spectra in the two types of damage. As a first attempt to study the impact of PKA energy on the results obtained in Fig. 2b, simulations were repeated with PKA energies of 5 and 10 keV. These simulations showed qualitatively similar results to Fig. 2b and results are therefore not included in this study.

Neutron irradiation of metals also creates transmutation products such as hydrogen and helium [10], which can significantly influence damage accumulation by acting as traps for dislocation loops and nucleation sites for bubbles [38–41]. Although ion irradiation with both self-ions (causing cascade damage) and transmutation products such as hydrogen and helium has been carried out experimentally [42], developing truly equivalent conditions to neutron damage in this case is a very challenging problem. For a more complete review of challenges associated with simulating neutron irradiation with charged particles, see the recent paper by Was [43]. Despite these differences, the results of this study show that the relationship between displacement rate and temperature alone is a primary variable for consideration when designing experiments using ion irradiation to simulate neutron damage.

The methodology proposed here is most appropriate when designing experiments in which the majority of damage accumulation occurs in the grain or thin film interior, rather than at grain boundaries. For irradiation at high temperatures and/or low displacement rates, significant damage accumulation can occur at grain boundaries and triple junctions [44–46], which are not included in this model. The framework developed here could be extended to systems containing internal defects including grain boundaries if a greater understanding of damage accumulation on such structures is achieved. In addition, neutron irradiation generates gases such as helium and hydrogen through transmutation which can influence damage accumulation [3,10,47,48]. Some experimental techniques include concurrent heavy ion irradiation and light ion implantation [42,49–52], making experimental investigation of these phenomena possible. Equivalence between these more complicated scenarios could be investigated by expanding this methodology to include helium and hydrogen in the SRSCD simulations. Stochastic cluster dynamics simulations of triple beam irradiation have been implemented by others [17,53], but the relationship between temperature and dose rate has not been investigated in these studies.

Finally, the results shown in Fig. 2 for Frenkel pairs and cascades

at 10^{-2} dpa assume the same total displacement in the 'target' and 'proxy' conditions, but the computed value of ΔT_P may change as the total radiation dose increases. Previous studies of the effect of displacement rate on damage accumulation during cascade implantation have shown that damage accumulation at varying displacement rates is similar above 10^{-2} dpa due to overlapping cascades [54], indicating that the temperature shift ΔT_P required at higher doses may decrease. This effect was not investigated in this work due to computational limitations, but deserves treatment in future studies.

Previous theoretical studies have investigated the relationship between displacement rate and temperature [2,4,13,14]. In the work of Mansur [14], a preliminary model is presented that includes only single vacancies and single interstitials. This scheme does not account for effects such as defect clustering, displacement cascades, or spatially resolved microstructures. Abromeit [4] addressed some of these limitations by creating a rate theory model that includes defect cluster populations, but the problem is not applied to a specific material and trends related to mechanisms for defect accumulation as a function of displacement rate are discussed instead. In the model of Short et al. [13], spatially resolved damage accumulation in thin films is simulated using displacement profiles from SRIM simulations, allowing investigation of 'neutron-atypical' effects such as void formation near the free surface of the thin film during charged particle irradiation. However, this study also does not include defect cluster formation or displacement cascades and does not investigate temperature shifts necessary to simulate neutron damage using charged particle irradiation. In the work of Xu et al. [15], many of these limitations have been addressed by including a complex cluster dynamics model with depth dependence and defect production rates based on PKA spectra of both neutron and ion damage. This study takes a similar approach to the work of Xu et al., including a detailed rate theory-based damage evolution model and inclusion of cascade damage. Although complex PKA spectra are not included in this work, a much larger input space of dose rates is treated.

5. Conclusions

In this study, the relationship between displacement rate and temperature are investigated for radiation defect accumulation in irradiated α-Fe under several irradiation conditions using the SRSCD simulation framework. The results of this analysis show that:

1. For irradiation of iron at 20 °C and 200 °C over a wide range of displacement rates and damage conditions such as damage type and material microstructure, an equivalent displacement rate and temperature pair can be found which provides similar defect accumulation results. This result is in agreement with the recent modeling work of Xu et al. [15].
2. The temperature shift ΔT_P required during irradiation at a 'proxy' displacement rate ϕ_P in order to produce similar radiation damage accumulation to irradiation at a 'target' displacement rate ϕ_T is not simply a function of the difference in displacement rates. Rather, ΔT_P is shown in this work to depend on both ϕ_T and ϕ_P as well as the radiation damage type (Frenkel pair or cascade damage) and reference temperature T_T. Film thickness is not shown to strongly influence ΔT_P for the limited irradiation conditions studied.

The methodology described here represents a preliminary step that can be used during experimental design in order to best reproduce radiation damage expected in irradiation conditions that are difficult to achieve in the laboratory, such as low displacement rate irradiation with neutrons.

Acknowledgments

This work is supported by the Sandia National Laboratories/Georgia Tech Excellence in Engineering Research Program.

This work is also supported by the US Department of Energy's Nuclear Energy University Program (DE-NE0000678).

Sandia National Laboratories is a multi-program laboratory managed and operated by Sandia Corporation, a wholly owned subsidiary of Lockheed Martin Corporation, for the U.S. Department of Energy's National Nuclear Security Administration under contract DE-AC04-94AL85000.

Appendix A. Migration and binding parameters of defects in α-Fe

Table A.1 shows the list of migration and binding parameters used in this study for point defects and clusters. Values are taken from atomistic studies [22,24]. This set of parameters controlling defect behavior has been used in previous studies using SRSCD and have been validated by comparison to experimentally measured defect accumulation [20].

Table A.1
Migration and binding parameters used in SRSCD simulations.

Migration parameters	$D = D_0 e^{-\frac{E_m}{k_b T}}$	
Single vacancy	$E_m = 0.67$ eV, $D_0 = 8.2 \times 10^{11}$ nm^2/s	[24]
2-*v* cluster	$E_m = 0.62$ eV, $D_0 = 8.2 \times 10^{11}$ nm^2/s	[24]
3-*v* cluster	$E_m = 0.35$ eV, $D_0 = 8.2 \times 10^{11}$ nm^2/s	[24]
4-*v* cluster	$E_m = 0.48$ eV, $D_0 = 8.2 \times 10^{11}$ nm^2/s	[24]
Larger *v* clusters	(immobile)	
Single interstitial	$E_m = 0.34$ eV, $D_0 = 8.2 \times 10^{11}$ nm^2/s	[24]
2-*i* cluster	$E_m = 0.42$ eV, $D_0 = 8.2 \times 10^{11}$ nm^2/s	[24]
3-*i* cluster	$E_m = 0.43$ eV, $D_0 = 8.2 \times 10^{11}$ nm^2/s	[24]
4-*i* cluster	$E_m = 0.43$ eV, $D_0 = 8.2 \times 10^{11}$ nm^2/s	[24]
n-*i* cluster (1D)	$E_m = 0.06 + 0.11(n^{-1.6})$, $D_0 = (3.5 \times 10^{10} + 1.7 \times 10^{11} n^{-1.7})$ nm^2/s	[22]
Binding energies		
$V_2 \rightarrow V + V$	$E_b = 0.3$ eV	[24]
$V_3 \rightarrow V_2 + V$	$E_b = 0.37$ eV	[24]
$V_4 \rightarrow V_3 + V$	$E_b = 0.62$ eV	[24]
Vacancy clusters ($n > 4$)	$E_b^v(n) = 2.07 - 3.01\left(n^{\frac{2}{3}} - (n-1)^{\frac{2}{3}}\right)$	[24]
$I_2 \rightarrow I + I$	$E_b = 0.8$ eV	[24]
$I_3 \rightarrow I_2 + I$	$E_b = 0.92$ eV	[24]
Interstitial clusters ($n > 3$)	$E_b^i(n) = 3.77 - 5.05\left(n^{\frac{2}{3}} - (n-1)^{\frac{2}{3}}\right)$	[24]

Appendix B. Discussion of irregularity in results due to statistical fluctuations

In this section, the source of statistical fluctuations in the results shown in Figs. 2b and 4 will be discussed. To aid in this discussion, the raw data used to generate Fig. 2 is shown in the Fig. B.7, with the concentration of vacancy defects (vacancies and vacancy clusters) given as a function of temperature and displacement rate. These plots are converted into the plots shown in Fig. 2 using the method shown in Fig. 1. The contours of the plots in Fig. B.7 represent iso-curves along which all displacement rate/temperature pairs produce the same vacancy defect concentrations.

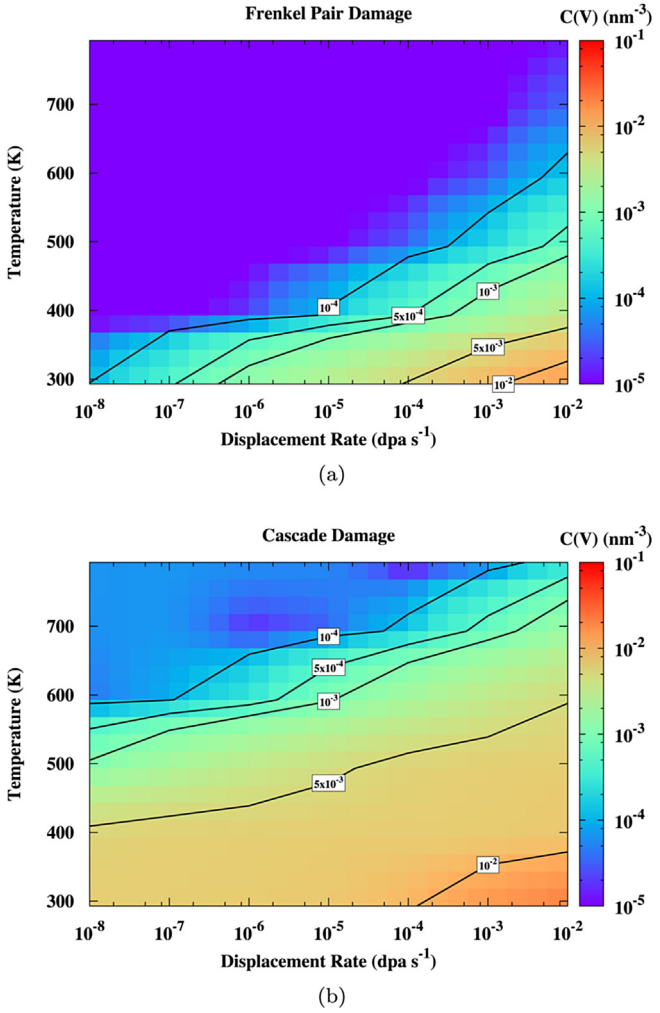

Fig. B.7. Concentration of vacancy defects (vacancies and vacancy clusters) for simulation conditions described in Section 3.1. Results are shown for Frenkel pair (B.7a) and cascade (B.7b) damage. This data is used to generate Fig. 2.

For the case of Frenkel pair irradiation, these contours are closely spaced, creating a steep gradient of increasing damage content with increasing displacement rate and decreasing temperature. However, for the case of cascade damage, these contours are more widely spaced and flatter, indicating a broad range of temperatures and dose rates in which similar damage content is produced. Therefore, estimation of the temperature shift required to match defect content at a given dose rate becomes more sensitive to the naturally occurring variations in defect concentrations produced by the SRSCD algorithm. This leads to the irregularities in the contour lines seen in Figs. 2b and 4, especially at 100 °C. It should be noted that values of (ϕ_T,ϕ_P) with larger uncertainty in ΔT_P due to the phenomenon described above are also regions in which damage accumulation is less sensitive to ΔT_P, making the precision of the estimate for ΔT_P less critical.

References

[1] G. Kinchin, R. Pease, The displacement of atoms in solids by radiation, Rep. Prog. Phys. 18 (1) (1955) 1.
[2] G.S. Was, Fundamentals of Radiation Materials Science: Metals and Alloys, Springer Science & Business Media, 2007.
[3] N. Packan, K. Farrell, J. Stiegler, Correlation of neutron and heavy-ion damage: I. the influence of dose rate and injected helium on swelling in pure nickel, J. Nucl. Mater. 78 (1) (1978) 143–155.
[4] C. Abromeit, Aspects of simulation of neutron damage by ion irradiation, J. Nucl. Mater. 216 (1994) 78–96.
[5] T. Muroga, H. Watanabe, N. Yoshida, Correlation of fast neutron, fusion neutron and electron irradiations based on the dislocation loop density, J. Nucl. Mater. 174 (2) (1990) 282–288.
[6] R. Nelson, D. Mazey, J. Hudson, The use of ion accelerators to simulate fast neutron-induced voidage in metals, J. Nucl. Mater. 37 (1) (1970) 1–12.
[7] M.J. Fluss, P. Hosemann, J. Marian, Charged-particle irradiation for neutron radiation damage studies, Charact. Mater. (2012) 1–17.
[8] J. Gan, G. Was, Microstructure evolution in austenitic fe–cr–ni alloys irradiated with rotons: comparison with neutron-irradiated microstructures, J. Nucl. Mater. 297 (2) (2001) 161–175.
[9] J. Mascitti, M. Madariaga, Method for the Calculation of Dpa in the Reactor Pressure Vessel of Atucha Ii, Science and Technology of Nuclear Installations, 2011.
[10] P. Vladimirov, S. Bouffard, Displacement damage and transmutations in metals under neutron and proton irradiation, Comptes Rendus Phys. 9 (3) (2008) 303–322.
[11] G. Was, J. Busby, T. Allen, E. Kenik, A. Jensson, S. Bruemmer, J. Gan, A. Edwards, P. Scott, P. Andreson, Emulation of neutron irradiation effects with protons: validation of principle, J. Nucl. Mater. 300 (2) (2002) 198–216.
[12] L. Mansur, Correlation of neutron and heavy-ion damage: ii. the predicted temperature shift if swelling with changes in radiation dose rate, J. Nucl. Mater. 78 (1) (1978) 156–160.
[13] M. Short, D. Gaston, M. Jin, L. Shao, F. Garner, Modeling injected interstitial effects on void swelling in self-ion irradiation experiments, J. Nucl. Mater. 471 (2015) 200–207.
[14] L. Mansur, Theory of transitions in dose dependence of radiation effects in structural alloys, J. Nucl. Mater. 206 (2) (1993) 306–323.
[15] D. Xu, G. VanCoevering, B.D. Wirth, Defect microstructural equivalence in molybdenum under different irradiation conditions at low temperatures and low doses, Comput. Mater. Sci. 114 (2016) 47–53.
[16] A.Y. Dunn, L. Capolungo, E. Martinez, M. Cherkaoui, Spatially resolved stochastic cluster dynamics for radiation damage evolution in nanostructured metals, J. Nucl. Mater. 443 (1) (2013) 128–139.
[17] J. Marian, V.V. Bulatov, Stochastic cluster dynamics method for simulations of multispecies irradiation damage accumulation, J. Nucl. Mater. 415 (1) (2011) 84–95.
[18] M. Li, M. Kirk, P. Baldo, D. Xu, B. Wirth, Study of defect evolution by tem with in situ ion irradiation and coordinated modeling, Philos. Mag. 92 (16) (2012) 2048–2078.
[19] A. Dunn, L. Agudo-Merida, I. Martin-Bragado, M. McPhie, M. Cherkaoui, L. Capolungo, A novel method for computing effective diffusivity: application to helium implanted α-fe thin films, J. Nucl. Mater. 448 (1) (2014) 195–205.
[20] A. Dunn, L. Capolungo, Simulating radiation damage accumulation in α-fe: a spatially resolved stochastic cluster dynamics approach, Comput. Mater. Sci. 102 (2015) 314–326.
[21] J.F. Ziegler, M.D. Ziegler, J.P. Biersack, Srim–the stopping and range of ions in matter, Nucl. Instrum. Methods Phys. Res. Sect. B Beam Interact. Mater. Atoms 268 (11) (2010) 1818–1823.
[22] N. Soneda, T. Diaz de La Rubia, Migration kinetics of the self-interstitial atom and its clusters in bcc fe, Philos. Mag. A 81 (2) (2001) 331–343.
[23] D. Terentyev, L. Malerba, P. Klaver, P. Olsson, Formation of stable sessile interstitial complexes in reactions between glissile dislocation loops in bcc fe, J. Nucl. Mater. 382 (2) (2008) 126–133.
[24] C.-C. Fu, J. Dalla Torre, F. Willaime, J.-L. Bocquet, A. Barbu, Multiscale modelling of defect kinetics in irradiated iron, Nat. Mater. 4 (1) (2005) 68–74.
[25] R. Stoller, G. Odette, B. Wirth, Primary damage formation in bcc iron, J. Nucl. Mater. 251 (1997) 49–60.
[26] R. Stoller, A. Calder, Statistical analysis of a library of molecular dynamics cascade simulations in iron at 100 k, J. Nucl. Mater. 283 (2000) 746–752.
[27] I. Martin-Bragado, A. Rivera, G. Valles, J.L. Gomez-Selles, M.J. Caturla, Mmonca: an object kinetic monte carlo simulator for damage irradiation evolution and defect diffusion, Comput. Phys. Commun. 184 (12) (2013) 2703–2710.
[28] M. Guseva, V. Gusev, U. Krasulin, Y.V. Martynenko, S. Das, M. Kaminsky, Radiation blistering of nb implanted sequentially with helium ions of different energies (3–500 kev), J. Nucl. Mater. 63 (1976) 245–252.
[29] M. Lewis, W. Allen, R. Buhl, N. Packan, S. Cook, L. Mansur, Triple ion beam irradiation facility, Nucl. Instrum. Methods Phys. Res. Sect. B Beam Interact. Mater. Atoms 43 (2) (1989) 243–253.
[30] E. Fu, A. Misra, H. Wang, L. Shao, X. Zhang, Interface enabled defects reduction in helium ion irradiated cu/v nanolayers, J. Nucl. Mater. 407 (3) (2010) 178–188.
[31] P. Ziemann, O. Meyer, G. Heim, W. Buckel, Low temperature self-ion irradiation of pure and granular aluminium-films, Z. für Phys. B Condens. Matter 35 (2) (1979) 141–149.
[32] I. Robertson, M. Kirk, W.E. King, Formation of dislocation loops in iron by self-ion irradiations at 40k, Scr. Metall. 18 (4) (1984) 317–320.
[33] I.-S. Kim, J. Hunn, N. Hashimoto, D. Larson, P. Maziasz, K. Miyahara, E. Lee, Defect and void evolution in oxide dispersion strengthened ferritic steels under 3.2 mev fe+ ion irradiation with simultaneous helium injection, J. Nucl. Mater. 280 (3) (2000) 264–274.
[34] M. Eldrup, B. Singh, S. Zinkle, T. Byun, K. Farrell, Dose dependence of defect accumulation in neutron irradiated copper and iron, J. Nucl. Mater. 307 (2002) 912–917.
[35] A. Marwick, The primary recoil spectrum in the simulation of fast-reactor radiation damage by charged-particle bombardment, J. Nucl. Mater. 55 (3)

(1975) 259–266.
[36] C.S. Becquart, A. Barbu, J. Bocquet, M. Caturla, C. Domain, C.-C. Fu, S. Golubov, M. Hou, L. Malerba, C. Ortiz, et al., Modeling the long-term evolution of the primary damage in ferritic alloys using coarse-grained methods, J. Nucl. Mater. 406 (1) (2010) 39–54.
[37] A. Souidi, M. Hou, C.S. Becquart, L. Malerba, C. Domain, R.E. Stoller, On the correlation between primary damage and long-term nanostructural evolution in iron under irradiation, J. Nucl. Mater. 419 (1) (2011) 122–133.
[38] L. Ventelon, B. Wirth, C. Domain, Helium–self-interstitial atom interaction in α-iron, J. Nucl. Mater. 351 (1) (2006) 119–132.
[39] K. Arakawa, R. Imamura, K. Ohota, K. Ono, Evolution of point defect clusters in pure iron under low-energy he+ irradiation, J. Appl. Phys. 89 (9) (2001) 4752–4757.
[40] K. Morishita, R. Sugano, B.D. Wirth, T.D. de La Rubia, Thermal stability of helium–vacancy clusters in iron, Nucl. Instrum. Methods Phys. Res. Sect. B Beam Interact. Mater. Atoms 202 (2003) 76–81.
[41] R. Barnes, D. Mazey, The migration and coalescence of inert gas bubbles in metals, in: Proceedings of the Royal Society of London a: Mathematical, Physical and Engineering Sciences, 275, The Royal Society, 1963, pp. 47–57.
[42] T. Tanaka, K. Oka, S. Ohnuki, S. Yamashita, T. Suda, S. Watanabe, E. Wakai, Synergistic effect of helium and hydrogen for defect evolution under multi-ion irradiation of fe–cr ferritic alloys, J. Nucl. Mater. 329 (2004) 294–298.
[43] G.S. Was, Challenges to the use of ion irradiation for emulating reactor irradiation, J. Mater. Res. 30 (09) (2015) 1158–1182.
[44] W. Han, M. Demkowicz, E. Fu, Y. Wang, A. Misra, Effect of grain boundary character on sink efficiency, Acta Mater. 60 (18) (2012) 6341–6351.
[45] B.N. Singh, T. Leffers, W. Green, M. Victoria, Nucleation of helium bubbles on dislocations, dislocation networks and dislocations in grain boundaries during 600 mev proton irradiation of aluminium, J. Nucl. Mater. 125 (3) (1984) 287–297.
[46] S.J. Zinkle, K. Farrell, Void swelling and defect cluster formation in reactor-irradiated copper, J. Nucl. Mater. 168 (3) (1989) 262–267.
[47] R.E. Stoller, The influence of helium on microstructural evolution: implications for dt fusion reactors, J. Nucl. Mater. 174 (2) (1990) 289–310.
[48] H. Ullmaier, The influence of helium on the bulk properties of fusion reactor structural materials, Nucl. Fusion 24 (8) (1984) 1039.
[49] A. Kohyama, Y. Katoh, M. Ando, K. Jimbo, A new multiple beams–material interaction research facility for radiation damage studies in fusion materials, Fusion Eng. Des. 51 (2000) 789–795.
[50] Y. Serruys, M.-O. Ruault, P. Trocellier, S. Henry, O. Kaïtasov, P. Trouslard, Multiple ion beam irradiation and implantation: jannus project, Nucl. Instrum. Methods Phys. Res. Sect. B Beam Interact. Mater. Atoms 240 (1) (2005) 124–127.
[51] K. Hattar, D.C. Bufford, D.L. Buller, Concurrent in situ ion irradiation transmission electron microscope, Nucl. Instrum. Methods Phys. Res. Sect. B Beam Interact. Mater. Atoms 338 (2014) 56–65.
[52] C. Chisholm, K. Hattar, A.M. Minor, In situ tem concurrent and successive au self-ion irradiation and he implantation, Mater. Trans. 55 (3) (2014) 418–422.
[53] T.L. Hoang, J. Marian, V.V. Bulatov, P. Hosemann, Computationally-efficient stochastic cluster dynamics method for modeling damage accumulation in irradiated materials, J. Comput. Phys. 300 (2015) 254–268.
[54] A. Dunn, R. Dingreville, L. Capolungo, Multi-scale simulation of radiation damage accumulation and subsequent hardening in neutron-irradiated α-fe, Model. Simul. Mater. Sci. Eng. 24 (1) (2015) 015005.